

Biomechanical proposal as a cause of incomplete seed and pericarp development of the sunflower (*Helianthus annuus* L.) fruits

Propuesta biomecánica como causa del desarrollo incompleto de la semilla y el pericarp de los frutos de girasol (*Helianthus annuus* L.)

Hernández LF^{1,2}, PM Bellés³, MA Bidegain^{4,5}, PD Postemsky⁴

Abstract. Absence or underdevelopment of sunflower fruits come usually from failure in fertilization, stresses as well as physiological and morphological defects in the ovary. Thigmomorphogenesis has never been included as a possible cause. We have previously shown that a 2-3 day fertilization shift can occur between neighboring florets in the sunflower capitulum. It is proposed here that those ovaries with advanced fertilization can generate a significant radial and axial compressive stress on ovaries with delayed fertilization. This mechanical stimulus could be strong enough to trigger a thigmo response that affects further ovary development. In vivo tests were performed, isolating ovaries by removing the adjacent flowers and rubbing them several times using a micromanipulator applying a force of 1 to 3 N. Total peroxidases in treated and untreated ovaries, isolated and not isolated were measured 24 h after treatments. Ovary development was studied in control and isolated flowers, both rubbed and not rubbed. Also a mechanical model was made to simulate the mechanical behavior of an ovary surrounded by advanced growing neighboring ovaries. A meshed 3-D model of a young ovary was constructed and a computer simulation was performed using finite element analysis. Shear stresses generated by the friction of neighboring ovaries in contact with the model, fertilized three days later, were then estimated. After rubbing, isolated ovaries *in planta* showed a thigmo response that resulted in empty or incompletely developed fruits. Total peroxidase levels ($\Delta\text{Abs}_{470} \text{ min}^{-1} \cdot \text{g fresh weight}^{-1}$) rose from 22 in control ovaries to 72 in rubbed ones. The number of ovaries that did not develop any seed from these incompletely developed fruits rose from 16.2 to 20.0% in the control non-isolated flowers to 61.1 to 86.7% in the rubbed ovaries, but dropped to 6.7 to 7.3% in the non-rubbed but isolated ovaries. From the simulation it was found that the area of contact with the receptacle was prone

Resumen. La ausencia o el escaso desarrollo de los frutos del girasol proviene generalmente de fallas en la fertilización, condiciones de estrés y defectos fisiológicos y morfológicos en el ovario. La tigmomorfogénesis nunca ha sido considerada como una posible causa. Hemos demostrado previamente que, en el capítulo de girasol, puede producirse un retraso de 2 a 3 días en la fertilización entre flores vecinas. En este trabajo se propone que los ovarios con fertilización avanzada pueden generar un significativo estrés compresivo radial y axial en los ovarios con fertilización retrasada. Este estímulo mecánico podría ser lo suficientemente importante como para desencadenar una thigmo respuesta que afecte el desarrollo de los ovarios. Se realizaron pruebas in vivo, aislando ovarios, eliminando las flores adyacentes y, usando un micromanipulador, frotándolas aplicando una fuerza de 1 a 3 N. Se midieron las peroxidases totales en los ovarios tratados y no tratados, aislados y no aislados 24 h después de los tratamientos. El desarrollo de los ovarios se estudió en flores control y aisladas, tanto frotadas como no frotadas. También se simuló el comportamiento mecánico de un ovario rodeado por ovarios vecinos en crecimiento avanzado. Para ello se construyó un modelo tridimensional mallado de un ovario joven y se realizó una simulación computacional utilizando el método de elementos finitos. Se estimaron las tensiones de corte generadas por la fricción de los ovarios vecinos fertilizados tres días antes y en contacto con el ovario con fertilización retrasada. En los tratamientos de fricción *in planta*, los ovarios aislados mostraron un desarrollo anómalo del embrión, resultando en frutos vacíos o incompletamente desarrollados. Los niveles totales de peroxidases ($\Delta\text{Abs}_{470} \text{ min}^{-1} \cdot \text{g peso fresco}^{-1}$) aumentaron de 22 en los ovarios control a 72 en los frotados. El número de ovarios que no desarrollaron semilla aumentó de 16.2 a 20.0% en las flores control no aisladas a 61.1 a 86.7% en las flores con ovarios frotados, pero disminuyó de 6.7 a 7.3% en las no flores no frotadas

¹ Laboratorio de Morfología Vegetal. Departamento de Agronomía, Universidad Nacional del Sur (UNS), 8000 Bahía Blanca.

² Comisión de Investigaciones Científicas de la Provincia de Buenos Aires (CIC), 1900 La Plata.

³ Depto. de Ingeniería, UNS, 8000 Bahía Blanca.

⁴ Centro de Recursos Renovables de la Zona Semiárida (CERZOS), UNS, CONICET, Lab. de Biotecnología de Hongos Comestibles y Medicinales, 8000 Bahía Blanca.

⁵ Departamento de Biología, Bioquímica y Farmacia, UNS, 8000 Bahía Blanca. Argentina.

Address correspondence to: Luis F. Hernández, e-mail: lfhernandez@uns.edu.ar

Received 28.V.2017. Accepted 5.VII.2018.

to show a higher magnitude of stress after deformation induced by shear forces generated by neighboring ovaries. Thigmomorphogenesis can also explain the failures observed at early stages of the sunflower ovary development. The ovary tissue sensitivity at this stage could contribute to the rapid response of the mechanically generated stimulus between neighbouring ovaries.

Keywords: *Helianthus annuus* L.; Finite element analysis; Ovary development; Peroxidase; Thigmo response.

pero con ovarios aislados. A partir de la simulación se encontró que la región de unión del ovario con el receptáculo era proclive a mostrar una mayor magnitud de estrés después de la deformación inducida por las fuerzas de fricción generadas por los ovarios vecinos. Se concluye que la tigmomorfogénesis puede también explicar en algunos casos las fallas observadas en las primeras etapas del desarrollo de los ovarios de girasol. La sensibilidad del tejido ovárico en esta etapa podría contribuir a la respuesta rápida del estímulo mecánico generado por fricción natural entre ovarios vecinos.

Palabras clave: Análisis de elementos finitos; Desarrollo del ovario; *Helianthus annuus* L.; Peroxidasa; Tigmo respuesta.

INTRODUCTION

Cultivated sunflower [*Helianthus annuus* L., var. *Macrocarpus* (D.C.) (Ckll)] is a very important crop for the production of vegetable oil in temperate regions of Argentina. The total number of fruits (achenes) per plant that fully develop seed (kernel) is one of the main yield components for both seed and oil production (Connor & Hall, 1997).

At maturity, the sunflower head (capitulum) usually shows a set of fruits with different degrees of hull (pericarp) and embryo (seed) development. In most of them, the embryo reaches its full size filling the internal ovary cavity (locule). These fruits are defined as fully developed (FDF) (Lindström et al., 2006; 2007). However, many mature fruits often contain ovules that did not fully develop into seeds. In those fruits, seed growth has stopped at different developmental stages, leaving them with an incompletely developed pericarp and/or seed. Even though the embryo has reached a certain level of development in many of them (Alkio et al., 2003; Lindström et al., 2004) they are usually named as “seedless”, “empty” or incompletely developed (IDF; Lindström et al., 2004). They can easily be identified in a mature capitulum because the hull is compressed by neighboring fruits and it shows an usually abnormal and collapsed pericarp (Fig. 1a-b).

The real causes of the origin of IDF are unknown but several proximate mechanisms that have been put forth to explain the low seed to ovule ratio in many species of the *Angiospermae* can be applied to this case. Then, the origin of IDF is usually attributed to environmental, physiological and/or anatomical causes, as well as lack of pollination or post pollination failures during the early development of the embryo (Birch & van der Sandt, 1985; Gillaspay et al., 1993; Connor & Hall, 1997; Cantagallo et al., 2004; Hernández & Bellés, 2005; Hernández, 2008). Also, competition for resources between developing ovaries, or vascular deficiencies at the ovary-receptacle interphase, have been proposed (Durrieu et al., 1985; Hernández & Orioli, 1991; Alkio & Grimm, 2003).

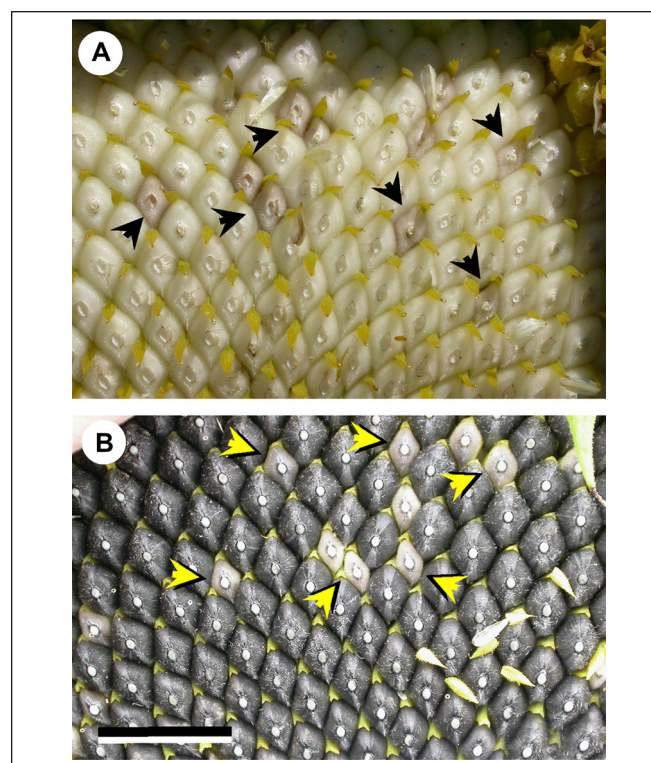


Fig. 1. (A) Peripheral region of the sunflower capitulum 10-15 DAFA (reproductive stage (RS) 6-7; Schneiter & Miller, 1981) showing delayed developed fruits (arrows), surrounded by advanced developed fruits. (B) The same region of Fig. 1A at RS9, 38 DAFA (physiological maturity). Arrows indicate the location of the pre-defined IDF observed in Fig. 1A. Note the fruits with smaller and lighter colored pericarps in comparison with those surrounding them. DAFA: days after anthesis. IDF: incompletely developed fruits. The scale bar for both figures is 1 cm.

Fig. 1. (A) Región periférica del capítulo del girasol 10-15 DAFA (estado reproductivo (RS) 6-7; Schneiter y Miller, 1981) mostrando frutos desarrollados retrasados (flechas), rodeados de frutos desarrollados avanzados. (B) La misma región de la Fig. 1A en RS 9, 38 DAFA (madurez fisiológica). Las flechas indican la ubicación de IDF predefinidos y presentados en la Fig. 1A. Observe los frutos con pericarpos más pequeños y más claros en comparación con los que los rodean. DAFA: días después de la antesis. IDF: frutos con desarrollo incompleto. La escala en ambas figuras = 1 cm.

Since the existence of IDF is the cause of a significant reduction in seed and oil production of sunflower, determining the causes of its origin is an important goal in studies of sunflower breeding.

A biomechanical point of view for the origin of IDF. Fruit development in the close-packed arrangement of ovaries of the sunflower capitulum during maturation can be viewed globally as a sum of the asymmetric compression and tractive forces exerted on the sidewalls between neighboring ovaries that permanently interact with each other. These forces can vary through time and even become dissipated during receptacle expansion (Hernández & Palmer, 1988, Hernández, 2015).

A detailed study of the visit path pattern of diurnal pollinators in sunflower, starting from the reproductive stage R5 (Schneider & Miller, 1981), showed a significant negative correlation ($R^2 = -0.61$; $P < 0.05$) between the capitulum florets covered by bee foraging paths (BFP) and the total IDF counted in the capitulum (Hernández, 2008).

Low pollinator visitation (0-30% BFP) resulted in poor seed set and IDF percentages ranging from 10 to 17%. Better pollinator visitation (60 to 90% BFP) diminished the number of IDF to 5 to 9%. An important irregular pattern of pollinator visits for a determined floret cluster was observed and it was concluded that as much as 30% or more of the receptacle floret area must be covered by polli-

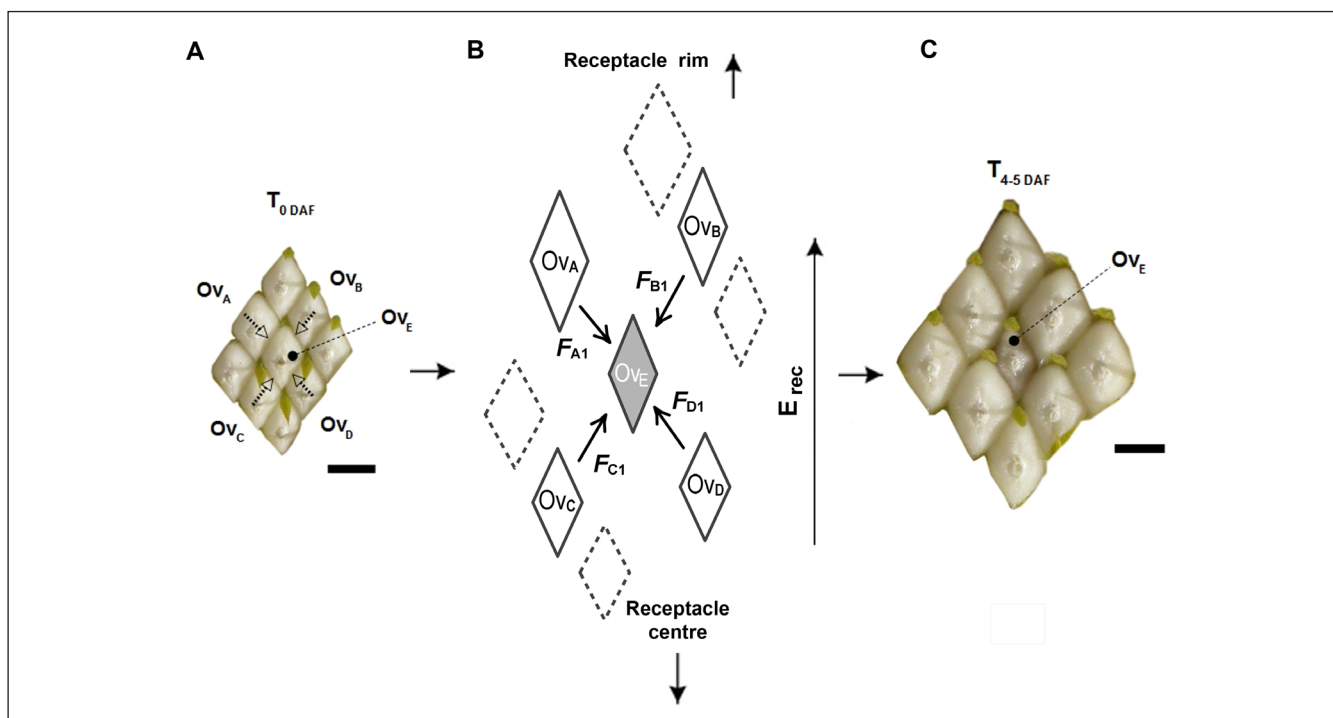


Fig. 2. Description of an ovary status with delayed fertilization and a biomechanical model of failure. (A) Initial status of the ovaries in a given capitulum sector before pollination (initial time; T_0 DAF). The ovary chosen for the model (Ov_E) presents a delay in pollination compared with its neighboring ovaries (ovaries Ov_A - Ov_D). When these ovaries start growing they exert tensions and pressures (dashed lined arrows) that are not compensated. (B) Schematic representation of the conceptual model of receptacle radial expansion and ovary growth on spatial competition. This is a simplified model of ovary growth from the point of view of forces interacting during the development of a given delayed growing ovary on the receptacle surface. While the whole receptacle is expanding radially, each growing ovary deals with competition for space with its neighbors. Ov_A - E : ovaries; F_A - D : direction of expansion forces exerted by neighboring ovaries. Neighboring ovaries developmental age is not the same because their relative position in the receptacle, then $F_B > F_A > F_D > F_C$. E_{rec} : receptacle radial expansion. (C) Five to seven days after the neighboring adjacent ovaries have been pollinated/fertilized (T_{4-5} DAF), the central ovary (Ov_E) is collapsed and with a relative size significantly smaller than those surrounding it.

Fig. 2. Descripción de un estado de ovario con fertilización retrasada y el modelo biomecánico de falla. (A) Estado inicial de los ovarios en un sector del capítulo antes de la polinización (tiempo inicial; T_0 DAF). El ovario elegido para el modelo (Ov_E) presenta un retraso en la polinización en comparación con los ovarios vecinos (ovarios Ov_A - Ov_D). Cuando estos ovarios comienzan a crecer, ejercen tensiones y presiones (flechas alineadas discontinuas) que no se compensan. (B) Representación esquemática del modelo conceptual de expansión radial de un receptáculo y crecimiento de ovarios compitiendo por espacio. Este es un modelo simplificado del crecimiento de un ovario desde el punto de vista de las fuerzas que interactúan durante el desarrollo del mismo con crecimiento retrasado. Mientras que todo el receptáculo se expande radialmente, cada ovario en desarrollo compite por espacio con sus vecinos. Ov_A - E : ovarios; F_A - D : dirección de las fuerzas de expansión ejercidas por los ovarios vecinos. El tiempo de desarrollo de los ovarios vecinos no es el mismo para todos debido a su posición relativa en el receptáculo, luego $F_B > F_A > F_D > F_C$. E_{rec} : expansión radial del receptáculo. (C) Cinco a siete días después que los ovarios vecinos adyacentes hayan sido polinizados/fertilizados (T_{4-5} DAF), el ovario central (Ov_E) está colapsado y con un tamaño relativo significativamente más pequeño a los que lo rodean.

nator visits to minimize the development of IDF (Hernández, 2008). These results indicate that in a given cluster of florets and for a given period of time, some of them can be pollinated to undergo fecundation while others can still remain unpollinated.

The question addressed here is if a mechano-sensing mechanism (Braam & Davis, 1990; Braam, 1992; Jaffe et al., 2002) triggered during ovary development could play a role in the origin of IDF in the sunflower inflorescence. This could be caused by the stresses exerted by the early fertilized ovaries on the later fertilized ones, inducing them to diminish their final size or to abort (Harder & Prusinkiewicz, 2013). In growing ovaries, the close-packed florets will always show self-brushing. So, therefore it depends on whether some ovaries are at the same growing stage or there is a time lag between some of them that creates a more intense thigmo effect on ovary development.

In this study, it is proposed that a floret fertilization delay of 2 to 4 days (Fig. 2a) would be enough for the rapidly expanding fertilized ovaries to exert radial pressures and axial traction able to generate mechanical disturbances on the delayed ovaries (Fig. 2b). This brushing stimulus would induce the synthesis of endogenous regulators by a thigmo response, for example, pollen tube advancement, the rate of flower senescence or the incorporation of water and photo-assimilates into the ovary and embryo (Fig. 2c).

MATERIALS AND METHODS

Plant material and cultural techniques. The experiments were carried out at the Agronomy Department-UNSur, Bahía Blanca, Argentina (Lat. 38° 45' S; Long. 62° 11' W) over two growing seasons. A sunflower genotype (Morgan MG3), pro-

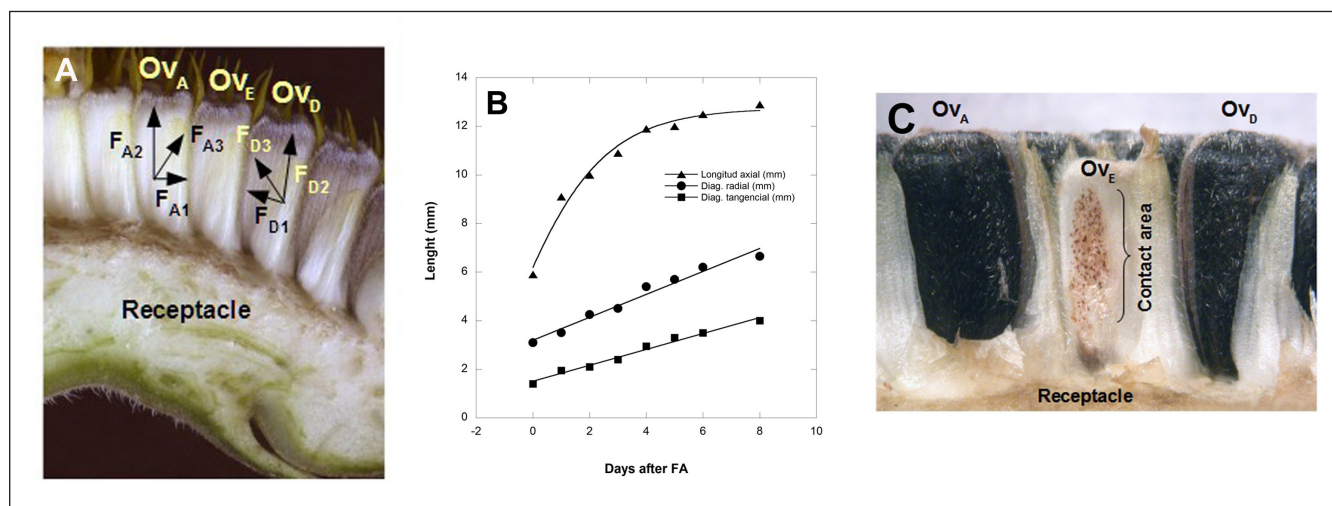


Fig. 3. (A) transverse section of the capitulum at RS 6, showing location of ovaries in the receptacle. In the figure, according to the hypothesis of the present study, two of the neighboring ovaries (OvA and OvD) that have been fertilized and started development exert radial pressures (FA3 and FD3) on the walls of the ovary with delay in fertilization (OvE). These ovaries also exert drag forces (FA2 and FD2), which are the result of the vectors of its axial (FA2) and radial (FA1) growth. (B) Mathematical fit of the dynamic analysis conducted on control fruits during 8 days after anthesis (DAFA), to measure the magnitude of the axial (▲), radial (●) and tangential (■) growth of the ovaries. Emerging rates of the adjustment equations were used in the FEM simulation:

Axial growth: Length (mm) = DAFA*1 - Exp((-1)*(0.047*(DAFA))^6.81)); R² = 0.951

Radial growth: Length (mm) = 3.2 + 0.8 x DAFA; R² = 0.982

Tangential growth: Length (mm) = 1.6 + 0.6 x DAFA; R² = 0.932

(C) Details of ovaries in RS 8 in a transverse section of the capitulum. The delayed growing ovary (OvE) is observed surrounded by the advanced growing ovaries (OvA and OvD). In ochre, the contact area between the ovaries is observed stained with safranin.

Fig. 3. (A) sección transversal del capítulo en el RS 6, mostrando la ubicación de los ovarios en el receptáculo. En esta Figura, de acuerdo con la hipótesis del presente estudio, dos de los ovarios vecinos (OvA y OvD) que se han fertilizado y comenzaron a desarrollarse ejercen presiones radiales (FA3 y FD3) en las paredes del ovario con retraso en la fertilización (OvE). Estos ovarios también ejercen fuerzas de fricción (FA2 y FD2), que son el resultado de los vectores de su crecimiento axial (FA2) y radial (FA1). (B) Ajuste del análisis dinámico realizado en frutos control durante 8 días después de la antesis (DAFA), para medir la magnitud del crecimiento axial (▲), radial (●) y tangencial (■) de los ovarios. Las tasas emergentes de las ecuaciones de ajuste se usaron en la simulación de elementos finitos (FEM):

Crecimiento axial: Longitud (mm) = DAFA*1 - Exp((-1)*(0.047*(DAFA))^6.81)); R² = 0.951

Crecimiento radial: Longitud (mm) = 3.2 + 0.8 x DAFA; R² = 0.982

Crecimiento tangencial: longitud (mm) = 1,6 + 0,6 x DAFA; R² = 0.932

(C) Detalles de los ovarios en RS8 en una sección transversal del capítulo. El ovario de crecimiento retardado (OvE) se observa rodeado por los ovarios en crecimiento avanzado (OvA y OvD). En ocre, el área de contacto entre los ovarios se observa teñida con safranina.

vided by Dow Agro of Argentina, was sown on three successive dates starting in the first week of October and separated by 7 days, to obtain plants at the beginning of flowering (first anthesis or reproductive stage (RS) 5.1, according to Schneider & Miller, (1981) during several consecutive days and study them individually.

This genotype was chosen because the external color of the fruit pericarp, white at early stages of fruit development and black-striate at maturity, makes the identification of IDF easy (Fig. 1a). At seedling emergence, plant density was adjusted to 6.0 plants/m². The crop was managed according to recommended conventional agronomical practices. Water was supplied by drip irrigation. Nutrient deficiencies were prevented with pre-planting and pre-flowering fertilization with nitrogen (60 kg N/ha) applied as NO₃K. Weeds were controlled manually. Insect pests were not an important factor throughout the whole growing season.

Analysis of the radial, tangential and axial expansion of adjacent ovaries. In 10 heads, 5 fertilized florets were identified and photographed from their fertilization (3 days after anthesis; DAFA) until R9 (38 DAFA) superimposing a millimeter scale. This allowed the measurement of the tangential and radial growth of the ovaries. Five adjacent ovaries, of the same age as the ones described above, were removed every two days during eight days to measure the rate of longitudinal growth (Fig. 3a). Results were adjusted by linear regression except for the axial growth of the fruit where the minimum square fit of the Gompertz equation was used (Fig.3b, Jukić et al., 2004). This allowed the rate of expansion of the ovary in two perpendicular and parallel axes to the surface of the receptacle to be defined.

Observation of the contact region between adjacent ovaries. Forces exerted by the ovaries on their narrow contact produce changes in the epidermis that can be identified with the dyeing of the cell walls that have undergone pressure due to contact (Fig. 3c). So, the scar tissue area caused by the contact surface between neighboring ovaries was determined in fruits at RS 8, by carefully removing the fruits and staining the surface with safranin solution which stains lignified, suberized, or cutinized cell walls (1% safranin in ethanol:distilled water 50% v/v; Ruzin, 1999). Each contact surface was photographed and then its area measured using *ImageJ* software (Rasband, 2016). Contact and free surfaces between adjacent ovaries were also studied by taking samples of the ovaries at RS6 and processing them for observation under a scanning electron microscopy. The samples were mounted on SEM holders using double-sided adhesive film and observed under a variable pressure scanning electron microscope (LEO, EVO 40-XVP. Cambridge, England, 2004) at 5 KV acceleration potential.

In vivo mechanical stimulation treatment on ovaries. Flowers from 2 to 3 DAFA were isolated by removing the



Fig. 4. A view of one capitulum where the treatment of post fertilization ovary isolation was conducted to determine its growth without the counteraction of the adjacent ovaries. In capitula with a similar treatment of ovary isolation in early stages of their growth, the rubbing treatment to simulate the effect of the growth was performed on the above mentioned ovary. The isolation was conducted by removing approximately 15-20 surrounding disc florets (Df) with tweezers and placing a plastic cylinder (Cyl) that avoided changes in forces in the isolated ovary (Ov) mainly produced by the extension of the receptacle and interaction with the rest of the florets. Phy: phyllaries.

Fig. 4. Una vista de un capítulo donde se realizó el tratamiento de aislamiento de ovarios después de la fertilización para determinar su crecimiento sin la contraracción de los ovarios adyacentes. En capítulos con un tratamiento similar de aislamiento de ovarios en las primeras etapas de su crecimiento, el tratamiento de frotamiento para simular el efecto del crecimiento se realizó en el ovario aislado (Ov) producidas principalmente por la extensión del receptáculo y la interacción con el resto de las flores. Phy: filarias.

adjacent flowers in the peripheral sector of the capitulum with tweezers (Fig. 4). The mechanical stimulation was conducted manually on isolated ovaries on the second day, following this protocol: individual ovaries were gently rubbed along the length of the ovary using an *ad hoc* micro-manipulator built with a professional compass. The pin end of the compass was fixed in the capitulum centre and a small pointed rod of silicone rubber 2.0 mm in diameter and 15.0 mm long was held on the opposite extreme. This process enabled the forces exerted on the ovary to be controlled without exceeding the limits tolerated by the point of attachment of the ovary (between 1 and 3 N; Sexton & Roberts, 1982; Yilmaz et al., 2011; Tata & Wien, 2014). Pressure exerted by hand was estimated, based on a previous assay conducted with the same procedure as that described for the ovaries but using an equipment for mechanical tests described by Hernández & Bellés (2007).

The treatments were: non-isolated florets (control), non-

rubbed isolated florets and stimulated isolated florets (rubbed). Fifty ovaries of each treatment in five plants were processed (10 ovaries per capitulum taken from the peripheral sector of each capitulum). Upon reaching RS9, the isolated and the mechanically treated ovaries and the controls were collected.

Soluble POD activity determination. Following the rubbing treatment (elapsed time: 70-75 h), ovaries from each treatment were collected by carefully removing them from the base in order to also take a partial portion of parenchymatic tissue from the receptacle. Samples were maintained at $-16\text{ }^{\circ}\text{C}$ until analysis.

POD enzyme activity was determined following the protocols from Cipollini (1998) with minor modifications. Briefly, preserved samples were ground using a chilled mortar and pestle in ice-cold 100 mmol/L sodium phosphate buffer pH 7.0 using a ratio of 5 mL buffer/g ovary fresh mass. Homogenates were centrifuged ($11600\times g$ for 15 min at $4\text{ }^{\circ}\text{C}$) and the cleared supernatant was analyzed for its soluble POD enzyme activity by following the formation of tetraguaiacol. Each reaction mixture (3 mL) consisted of 100 μL enzyme extract and 2.9 mL guaiacol solution (0.25% guaiacol by volume in 10 mmol/L sodium phosphate buffer pH 6.0) and 0.125% H_2O_2 (v/v). Results were expressed as the increase in

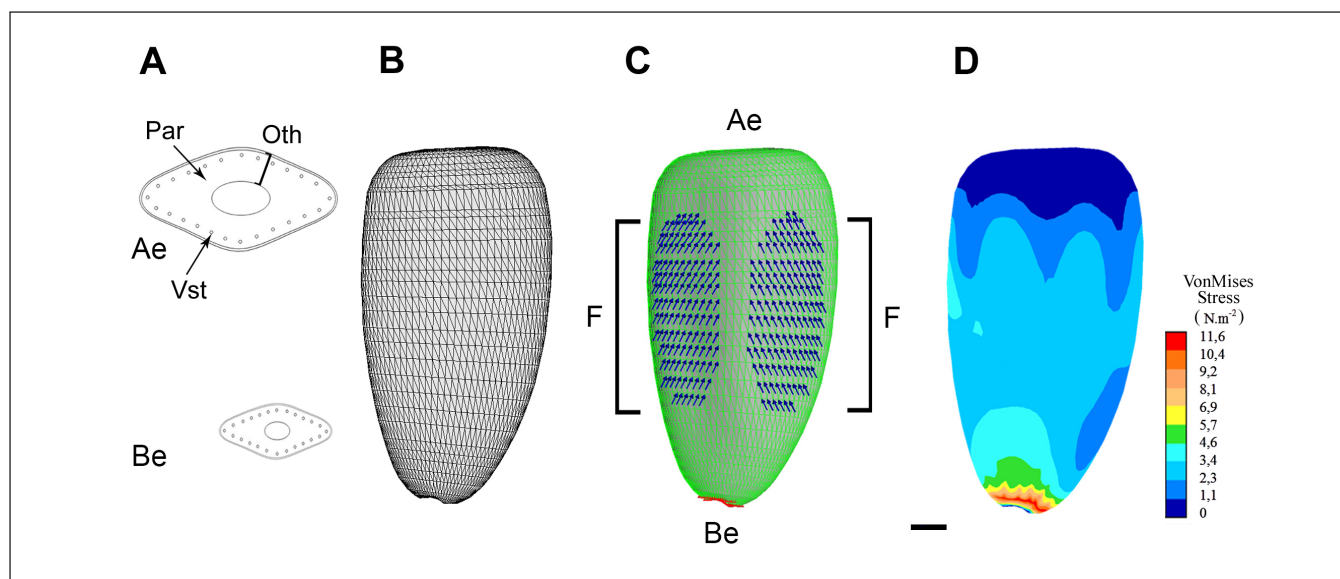


Fig. 5. (A) A transverse section of the ovaries at 3 DAFA, near the insertion zone with the receptacle (Be) and in the upper region, respectively (Ae). The 3-D model was constructed with the profile of these sections and the length of the ovary for the FEM simulation and also for calculation of its volume. To define the mechanical parameters in the simulation model, two structural materials were considered: parenchyma (Par) and the vascular traces (Vst). (B) Meshed model of a sunflower ovary after the integration of the coordinates in different planes of images taken from ovaries at 3 to 5 DAFA. (C) 3-D model used for MES. It was constructed as a uniaxial projection of the transverse section meshed model, considering an ovary wall of $200\text{ }\mu\text{m}$ thick (Oth). Lateral brushing forces from neighboring ovaries are noted with blue arrows (F). The shape of the region where these forces are applied in the model is taken from the observation of the contact areas between neighbor ovaries (Fig. 3C). The red mark at the bottom of the model denotes the region of ovary attachment to the receptacle surface. (D) Calculated stresses (vonMises, N/m^2) and its location in the ovary after the simulation. Note the higher stress values are close to the points of the ovary attachment to the receptacle. Color scale bar indicates gradient areas (from maximum, in red, to minimum, in blue) of VonMises stresses (N/m^2) in the simulation. Lateral forces in the simulation were acting during 1 min. Stress magnitudes are shown for longitudinal orientations. Bar for (A): $180\text{ }\mu\text{m}$; bar for (B-D): 1.0 mm .

Fig. 5. (A) Una sección transversal de los ovarios a 3 DAFA, cerca de la zona de inserción con el receptáculo (Be) y en la región superior, respectivamente (Ae). El modelo 3-D se construyó con el perfil de estas secciones y la longitud del ovario para la simulación con el FEM y también para el cálculo de su volumen. Para definir los parámetros mecánicos en el modelo de simulación, se consideraron dos materiales estructurales: parénquima (Par) y los haces vasculares (Vst). (B) Modelo de malla de un ovario de girasol después de la integración de las coordenadas en diferentes planos de imágenes tomadas de los ovarios a 3 a 5 DAFA. (C) Modelo 3-D utilizado para realizar la MES. Se construyó como una proyección uniaxial del modelo de malla de sección transversal, considerando una pared de ovario de $200\text{ }\mu\text{m}$ de espesor (Oth). Las fuerzas de fricción lateral de los ovarios vecinos se indican con flechas azules (F). La forma de la región donde se aplican estas fuerzas en el modelo se tomó de la observación de las áreas de contacto entre los ovarios vecinos (Fig. 3C). La marca roja en la parte inferior del modelo indica la región de unión de los ovarios a la superficie del receptáculo. (D) Estrés calculados (vonMises, N/m^2) y su ubicación en el ovario después de la simulación. Tener en cuenta que los valores de tensiones más altos se localizan en los puntos de contacto del ovario con en el receptáculo. La escala de colores indica el gradiente (desde el máximo, en rojo, hasta el mínimo, en azul) de las tensiones de VonMises (N/m^2) en la simulación. Las fuerzas laterales, en la simulación, actuaron durante 1 min. Las magnitudes de tensión se muestran solamente para orientaciones longitudinales. Escala en (A): $180\text{ }\mu\text{m}$; escala en (B-D): 1.0 mm .

absorbance at 470 nm \cdot min⁻¹ \cdot g fresh weight⁻¹ obtained at the linear phase of the enzyme reaction. The protein content was determined following the method of Bradford (1976) using bovine serum albumin as standard. All chemicals were from Sigma-Aldrich, St. Louis, Missouri, USA. Data were analyzed for each experiment with an Analysis of Variance using the software Infostat (DiRienzo et al., 2012).

Calculation and localization of stress in the model. Modeling and stress simulation. Stress at the site of the ovary/receptacle interface was calculated using the finite element method (FEM; Logan, 2001). This is a numerical procedure used for both static and dynamic structural analyses, suited for solving the partial differential equations which describe stresses and strains in structures that have heterogeneous properties, such as biological materials. The analysis was made using the ACCUPACK/VE routine from the FEM software Algor Simulation Professional (vers.11, Autodesk, Inc., San Rafael, CA; Hernández & Bellés, 2007), an FE software processor for non-linear calculation to conduct a mechanical event simulation (MES).

A 3-D model of the ovary was built based on the external shape of randomly selected ovaries of the studied genotype. Digital images of transversal and longitudinal sections of these ovaries were taken, and their contours obtained and saved as TIF files (Fig. 5a). The stack of digital contours was integrated in a 3-D model using the software 3D-Slicer (www.slicer.org, Kikinis et al., 2014). The model was saved as an STL file and imported into Blender (www.blender.org). The triangle meshed model was remodeled into rectangular patches when convenient and saved as a DXF file (Fig. 5b). This file was imported into the FEM software where the model was properly meshed (Fig. 5c) using the shell structural element (Logan, 2001; Hernández & Bellés, 2005; 2007). The shell-based surface is justified since the whole ovary is very thin compared with the in-plane dimensions. Three-nodal triangles and 4-nodal squares were used, giving the model a configuration of 2131 elements with 2080 nodes (Fig. 5c; Logan, 2001).

For the purpose of simplification and model definition the ovary was considered to be mainly composed of two tissues that were incorporated as two independent element groups, parenchyma (Par) and vascular traces (Vt) (Fig. 5a). Another two element groups were defined in order to give the model more realistic structural properties. They were the basal (Be) and apical (Ae) ovary ends (Fig. 5b). The ovary wall thickness (Oth) was measured on transverse sections at the median section (Fig. 5a). The ovule inside the ovary was not included. We consider that at this stage of development and regarding the hypothesis, the ovule provided little, if any, influence to the traction of the ovary walls. In this model, the material was modeled as an isotropic material, instead of a composite (Thibaut et al., 2001).

The bottom end of the ovary model (Fig. 5c) was fixed and stretching stresses during MES applying a displacement boundary condition ($F= 0.0$ to 1.0 N during 2.0 s) at the site of the external ovary walls were recorded at a capture rate of 130 steps/sec.

On the four faces of the ovary model, forces (noted as " F " in Fig. 5c) were applied by distributing them into four previously defined "contact areas" of neighboring ovaries identified in isolated ovaries that had previously been in contact with their neighbors (Fig. 3b).

Biomechanical properties in the model. Ovary wall thickness was measured from transverse sections made on fresh 3 DAFA ovaries (Fig 5a). Ovary wall tissue density was estimated from the weight of whole ovaries also 3 DAFA, and ovary volume. The last parameter emerged from the 3-D model loaded in the FEM software. So, the hull density in the ovary walls:

$$\delta_{\text{ovary walls}} (\text{g/cm}^3) = \text{Ovary fresh weight (g)} / \text{Ovary volume (cm}^3\text{)} \quad (\text{Table 1})$$

External dimensions and the relative proportions for each tissue estimated from the surface areas of each constitutive tissue were measured from transverse sections of the ovaries (Fig. 5a). With reference to the constitutive properties of biological materials, a significant amount of information is available in the literature. The Young's modulus of parenchyma and sclerenchyma, as well as their Poisson coefficients, were taken from the literature (Preston, 1974; Wainwright et al., 1982; Niklas, 1992). The Young's modulus of the vascular traces used in the model was from Hepworth & Vincent, (1998; Table 1).

Table 1. Mechanical properties assigned to the model and magnitude and orientation of the forces applied to it, to simulate a mechanical disturbance of neighboring fruits.

Tabla 1. Propiedades mecánicas asignadas al modelo y magnitud y orientación de las fuerzas aplicadas al mismo, para simular una perturbación mecánica de los frutos vecinos.

| Ovary physical parameters | Dimension |
|--|----------------|
| Elastic modulus (E ; kN) | 80.0 |
| Poisson coefficient (ν) | 0.36 |
| Wall thickness (μm) | 200.0 |
| Wall density (δ ; g/m^3) | 36.0 |
| Applied forces during the simulation (F , N) | 1.0 to 1.5 |
| Applied forces orientation during the simulation | Four sides (*) |

(*) On the four ovary sides, forces were tilted 10 degrees, as depicted in Fig. 5C.

(*) En los cuatro lados del ovario, las fuerzas están inclinadas 10 grados, como se muestra en la Fig. 5C.

RESULTS AND DISCUSSION

The development of the rubbed ovaries was significantly affected, with, 4 weeks after treatment (R8), a morphology similar to that of the IDF fruits previously described and an absent or very poorly developed embryo (Table 2).

Rubbing treatments also resulted in a significant increase in the activity of the soluble POD. This activity did not differ between the control ovaries (non-isolated) and untreated isolates (Table 2). The detection of POD activity was performed three days after treatments. It is unknown whether this response to rubbing persists over time, although there is evidence in other plant tissues that POD activity can be maintained up to 14 days after induction (Cipollini, 2002). If this is so, this response would surely have a significant negative effect on the development of the fruit, both in the pericarp and the embryo.

Studies on the local response of the thigmo stimulus have shown that the first sign of mechano-response is an increase in cytosolic calcium followed by the release of ethylene (Jaffe, 1973; Biro et al., 1980; Erner et al., 1980; Huberman & Jaffe, 1981; Biro & Jaffe, 1984). However, it has been stated that this hormone is unlikely to be involved in either the molecular or developmental responses of plants to mechanical stimuli. This conclusion is supported by observations that plants exposed to touch or shaking show a rapid (1 to 3 min) reduction in the rate of shoot elongation whereas ethylene release takes 30 to 45 min to be detected (Johnson et al., 1998).

It can clearly be seen that the position and the pattern of high von Mises (Meyers & Chawla, 2009) stress values in the FE model after MES corresponds to tensions located in the region of the ovary attachment to the receptacle (Fig. 5d). Moreover, the sequential results of the dynamic simulation show that at the initiation of the simulation, the highest stress values were observed in the region of the insertion point near the receptacle. Then, due to the asymmetry of the structure,

which is relatively lower in the insertion diameter than in the ovary apex (Fig. 5c), the stresses propagated acropetally (Fig. 5d).

The calculated vonMises stresses and their location on the ovary after simulation showed values between 6.5 to 11.6 N/m² that exceed the maximum limit of resistance of the constituent tissues located near the site of attachment of the ovary with the receptacle (Fig. 5d; Yilmaz et al., 2011).

The computed stress magnitudes, higher than 2 N/m², can be considered high enough to induce a thigmo morphogenic response (Jaffe et al., 1980; 2002) and this suggests the generation of a traction stress at that site which can trigger physical alterations at vascular tissue level and / or the induction of biochemical responses as a result of the mechanical disturbance (increase in POD enzyme activity; Table 2).

Rubbing between neighboring ovaries (Fig. 6) could incorporate another component in addition to the thigmo effect already defined (Takeda et al., 2013). In fact, SEM observations of the contact area with adjacent ovaries (Figs. 6a-b) compared with the basal region of the ovary where contact is minimal or absent (Figs. 6a and c), reveal wrinkled epidermal cells of the ovary with collapsed epidermic trichomes (Fig. 6b).

The non glandular epidermal trichomes of the ovary in Asteraceae present significant cell contents of terpenoids and polyphenols (Cornara et al., 2001; Aschenbrenner et al., 2013; Sulborska, 2013). The release of intracellular content from pressed trichomes could act as a localized regulator of the development of ovary walls (Bhushan Mandava, 1979; Zahra, 2012; Tholl, 2015).

On the other hand, formation of wrinkles or micro-fisures in the ovary epidermis as well as in the regions of attachment of the ovary to the receptacle, suggests that during ovary development a “stretching vascular tissue” is generated, particularly at the level of their insertion in the receptacle (Hervieux et al., 2016). This event could prevent the appropriate photo-assimilate flow from the receptacle to the flower after fertilization.

Table 2. Evaluation of embryo development in fruits at physiological maturity and content of soluble peroxidases (expressed on fresh weight) measured 3 days after rubbing treatments in the two seasons in which the experiments were carried out. RS (reproductive stage) 8, after Schneider and Miller 1981. Values followed by different letter, in each column, indicate the significance ($P < 0.05$) between treatments from the ANOVA statistical analysis.

Tabla 2. Evaluación del desarrollo del embrión en frutos con madurez fisiológica y contenido de peroxidases solubles (expresadas en peso fresco) medido 3 días después de los tratamientos de frotamiento en las dos estaciones en que se llevaron a cabo los experimentos. RS (estado reproductivo) 8, según Schneider y Miller 1981. Los valores seguidos letras diferentes, en cada columna, indican la significancia ($P < 0,05$) entre los tratamientos luego del análisis estadístico ANDEVA.

| TREATMENT | Fruits at RS8 with absent or incompletely developed embryo (n=15) (%) | | Soluble peroxidases in the whole ovary (n=50) ($\Delta\text{Abs}_{470} \text{ min}^{-1} \text{ g fresh weight}^{-1}$) | |
|-------------------------------|---|------------------------|---|------------------------|
| | 1 st season | 2 nd season | 1 st season | 2 nd season |
| Isolated ovaries | 6.7 a | 7.3 a | 21.7 ± 8.3 a | 19.0 ± 13.4 a |
| Isolated ovaries + rubbing | 86.7 b | 61.1 b | 71.8 ± 12.6 b | 27.7 ± 9.6 a |
| Control ovaries (undisturbed) | 20.0 c | 16.2 c | 22.2 ± 7.5 c | 23.2 ± 5.5 a |

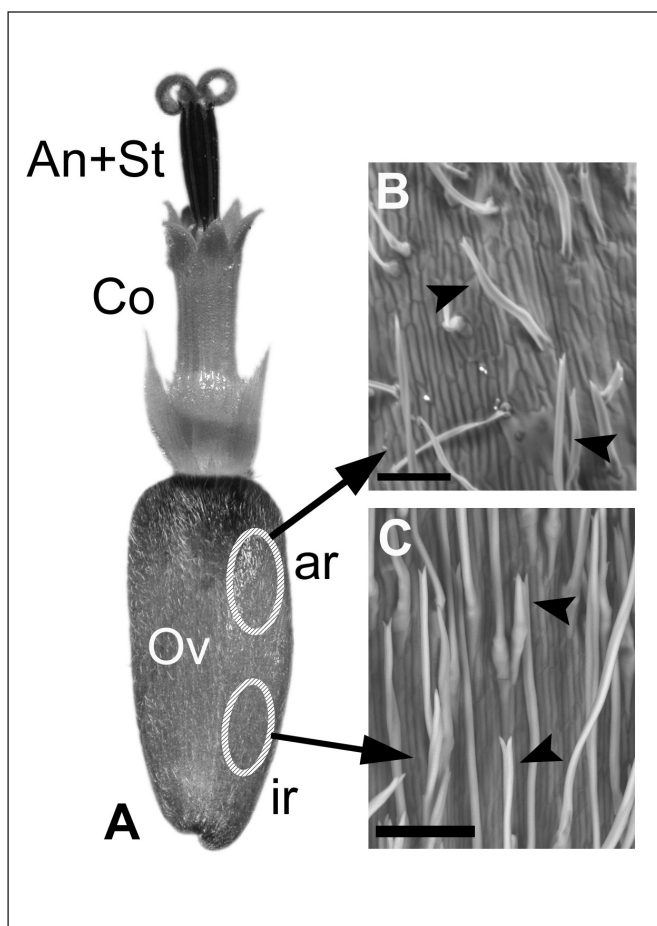


Fig. 6. (A) A control sunflower floret at RS6 sampled in its natural surrounding. In that context, mutual contact and pressures occur on the ovary surface. The above mentioned ovary is exposed to a gradient of forces of contact with its neighbors (See Fig. 2). These forces being of higher magnitude in the upper third area (Ar) and decreasing in a basipetal (lr) direction. (B) SEM micrograph of the ovary upper region. Note few epidermal cells collapsed or wrinkled. (C) SEM micrograph of the basal and intermediate region of the same ovary. In this case epidermal cells appear to be more conserved. In (B) and (C) the epidermis shows the abundance of twin hairs (arrows; Hess, 1938). Ov: ovary; Co: corolla; An: androecium. Ar: apical region; lr: inferior region. Scale bars: 100 μ m.

Fig. 6. (A) Una flor control de girasol en RS 6 tomada en su entorno natural, rodeada por el resto de las flores en el receptáculo. En ese contexto, el contacto y las presiones mutuas ocurren en la superficie del ovario. El ovario está entonces expuesto a un gradiente de fuerzas de contacto con sus vecinos (véase la Fig. 2). Estas fuerzas son de mayor magnitud en el área del tercio superior (Ar) y disminuyen en sentido basípeto (lr). (B). Microfotografía con SEM de la región superior del ovario. Se observa que pocas células epidérmicas están colapsadas o arrugadas. (C) Microfotografía con SEM de la región basal e intermedia del mismo ovario. En este caso, las células epidérmicas se muestran más conservadas. En (B) y (C), la epidermis muestra la abundancia de pelos gemelos (flechas; Hess, 1938). Ov: ovario; Co: corola; An: androceo. Ar: región apical; lr: región inferior. Barras: 100 μ m

The FE model described in this paper is a theoretical representation of the sunflower ovary, its constitutive tissues and their biomechanical properties and it is based on a realistic (though approximate) geometry. Since the aim of this study is to obtain qualitative results, the computed stresses can be considered as representative of a possible and real loading state of the sunflower ovary at an early stage of development.

It is known that plant developmental responses to mechanical stress involves the mechanical signal transduction associated with cell responses to the expression of TCH genes (Braam, 1992; Mauget et al., 1997) and the transfer of information from the site of perception to the sensitive sites where developmental processes are taking place (Braam & Davis, 1990; Depege et al., 1999; White & Broadley, 2003; Chehab et al., 2012).

In the present study, we have used an alternative approach for calculating the longitudinal and radial stresses at the ovary periphery. Our findings show that a possibility does exist for a gentle traction of advanced-fertilized ovaries on delayed ones, which could represent a mechanical stimulus able to perturb the normal fate of the ovary development.

ACKNOWLEDGEMENTS

This study is supported by the Secretaría Gral. de Ciencia y Tecnología (SeGCyT) UNS, the Comisión de Investigaciones Científicas de la Pcia. de Bs. As. (CIC), La Plata Argentina and the Consejo Nacional de Investigaciones Científicas y Técnicas (CONICET, Proyecto de Unidades Ejecutoras CERZOS 2017). Authors want to thank Prof. A. Flemmer for histological processing. We warrant that we have no conflict of interest to declare.

REFERENCES

- Alkio, M., A. Schubert, W. Diepenbrock & E. Grimm (2003). Effect of source-sink ratio on seed set and filling in sunflower (*Helianthus annuus* L.). *Plant, Cell and Environment* 26: 1609-1619.
- Alkio, M. & E. Grimm (2003). Vascular connections between therceptacle and empty achenes in sunflower (*Helianthus annuus* L.). *Journal of Experimental Botany* 54: 345-348.
- Aschenbrenner, A.K., S. Horakh & O. Spring (2013). Linear glandular trichomes of *Helianthus* (Asteraceae): morphology, localization, metabolite activity and occurrence. *AoB PLANTS*; 5 plt 028.
- Bhushan Mandava, N. (1979). Natural Products in Plant Growth Regulation. *Plant Growth Substances, ACS Symposium Series*, Vol. 111, Ch. 7, pp 135-213.
- Birch, E.B. & J.C van der Sandt (1985). Bee pollination of sunflower. *11th International Sunflower Conf. Proc.*, Mar del Plata, Argentina, ISA, pp. 255-260.
- Biro, R.L., J.R. Hunt, Y. Erner & M.J. Jaffe (1980). Thigmomorphogenesis: Changes in cell division and elongation in the internodes of mechanically perturbed or ethrel treated bean plants. *Annals of Botany* 45: 655-664.
- Biro, L.R. & M.J. Jaffe (1984). Thigmomorphogenesis: ethylene evolution and its role in the changes observed in mechanically perturbed bean plants. *Physiologia Plantarum* 62: 289-296.

- Braam, J. & R.W. Davis (1990). Rain-wind and touch-induced expression of calmodulin and calmodulin-related genes in *Arabidopsis*. *Cell* 60: 357-364.
- Braam, J. (1992). Touch-induced regulation of expression of the calmodulin-related TCH genes and thigmomorphogenesis in *Arabidopsis*. *Current Biotechnology Agriculture* 13: 82-95.
- Bradford, M. (1976). A rapid and sensitive method for the quantification of microgram quantities of protein using the principle of protein-dye binding. *Analytical Biochemistry* 72: 248-254.
- Cantagallo, J.E., D. Medan & A.J. Hall (2004). Grain number in sunflower as affected by shading during floret growth, anthesis and grain setting. *Field Crops Research* 85: 191-202.
- Chehab, E.W., C. Yao, Z. Henderson, S. Kim & J. Braam (2012). *Arabidopsis* touch-induced morphogenesis is jasmonate mediated and protects against pests. *Current Biology* 22: 701-706.
- Cipollini, D.F. (1998). The induction of soluble peroxidase activity in leaves of bean plants by wind-induced mechanical perturbation. *American Journal of Botany* 85: 1586-1591.
- Connor, D.J. & A.J. Hall (1997). Sunflower Physiology, pp. 113-182. In: Schneiter A.A. (Ed.), Sunflower Technology and Production, Agron. Ser. 35, ASA, CSSA, SSSA, Madison, WI, USA.
- Cornara, L., M. Bononi, F. Tateo, G. Serrato-Valenti & M.G. Mariotti (2001). Trichomes on vegetative and reproductive organs of *Stevia rebaudiana* (Asteraceae). Structure and secretory products. *Plant Biosystematics* 135: 25-37.
- Depege, N., C. Thonat, J.L. Julien & N. Boyer (1999). Thigmomorphogenesis: modifications of calmodulin mRNA and protein levels in tomato plants. *Journal of Plant Physiology* 155: 561-567.
- Di Rienzo, J.A., F. Casanoves, M.G. Balzarini, L. González, M. Tablada & C.W. Robledo (2012). *InfoStat* vers. 2012. Grupo InfoStat, FCA, Universidad Nacional de Córdoba, Argentina. URL: <http://www.infostat.com.ar>
- Durrieu, G., C. Percie du Sert & A. Merrien (1985). Anatomie du capitule de tournesol conséquences sur la nutrition des akènes. *11th International Sunflower Conf. Procs.*, Mar del Plata, Argentina, ISA, pp. 7-12.
- Erner, Y., R. Biro & M.J. Jaffe (1980). Thigmomorphogenesis: evidence for a translocatable thigmomorphogenetic factor induced by mechanical perturbation of beans (*Phaseolus vulgaris*). *Physiologia Plantarum* 50: 21-25.
- Gillaspy, G., H. Ben-David & W. Gruissem (1993). Fruits: a developmental perspective. *The Plant Cell* 5: 1439-1451.
- Harder, L.D. & P. Prusinkiewicz (2013). The interplay between inflorescence development and function as the crucible of architectural diversity. *Annals of Botany* 112: 1477-1493.
- Hepworth, D.G. & J.F.V. Vincent (1998). Modelling the mechanical properties of xylem tissue from tobacco plants (*Nicotiana tabacum* "Samsun") by considering the importance of molecular and micromechanisms. *Annals of Botany* 81: 761-770.
- Hernández, L.F. & J.H. Palmer (1988). A computer program to create the Fibonacci floret pattern on the sunflower head. *12th International Sunflower Conf. Procs.*, Novi Sad, Yugoslavia, ISA, pp. 150-155.
- Hernández, L.F. & G.A. Orioli (1991). Role of different leaves of the sunflower (*Helianthus annuus* L.) plant during the grain filling period (in Spanish). *Turrialba* 41: 330-334.
- Hernández, L.F. & P.M. Bellés (2005). Occurrence of incompletely developed fruits in the sunflower capitulum. Biomechanical approach to explain its causes (in Spanish). *III Argentine Sunflower Association Meeting*, Buenos Aires, Argentina, ASAGIR, pp. 12-14.
- Hernández, L.F. & P.M. Bellés (2007). A 3-D finite element analysis of the sunflower (*Helianthus annuus* L.) fruit. Biomechanical approach for the improvement of its hullability. *Journal of Food Engineering* 78: 861-869.
- Hernández, L.F. (2008). Visit path pattern of the honeybee (*Apis mellifera* L.) on the sunflower capitulum. Correspondence with the location of seedless and incompletely developed fruits. *Helia* 31: 1-16.
- Hernández, L.F. (2015). Spatial constraints also regulates final achene mass in the sunflower (*Helianthus annuus* L.) capitulum. *International Journal of Plant Biology* 6: 37-42.
- Hervieux, N., M. Dumond, A. Sapala, A.L. Routier-Kierzkowska, D. Kierzkowski, A.H.K. Roeder, R.S. Smith, A. Boudaoud & O. Hamant (2016). A Mechanical feedback restricts sepal growth and shape in *Arabidopsis*. *Current Biology* 26: 1019-1028.
- Huberman, M. & M.J. Jaffe (1981). Morphological changes of mechanically-perturbed or ethylene treated bean plants. *Plant Physiology* 67 (suppl.):17.
- Jaffe, M.J. (1973). Thigmomorphogenesis: The response of plant growth and development to mechanical stimulation. *Planta* 114: 143-157.
- Jaffe, M.J., R. Biro & K. Bridle (1980). Thigmomorphogenesis: calibration of the parameters of the sensory function in beans. *Physiologia Plantarum* 49: 410-416.
- Jaffe, M.J., A.C. Leopold & R.C. Staples (2002). Thigmo responses in plants and fungi. *American Journal of Botany* 83: 375-382.
- Johnson, K.A., M.L. Sistrunk, D.H. Polisensky & J. Braam (1998). *Arabidopsis thaliana* responses to mechanical stimulation do not require ETR1 or EIN2. *Plant Physiology* 116: 643-649.
- Jukic, D., G. Kralik & R. Scitovskia (2004). Least-squares fitting Gompertz curve. *Journal of Computational and Applied Mathematics* 169: 359-375.
- Kikinis, R., S.D. Pieper & K. Vosburgh (2014). 3D Slicer: a platform for subject-specific image analysis, visualization, and clinical support. *Intraoperative Imaging Image-Guided Therapy* 3: 277-289.
- Lindström, L.I., M.E. García & L.F. Hernández (2004). Morphology and distribution of incompletely developed fruits in sunflower (*Helianthus annuus* L.) capitulum. *17th International Sunflower Conf. Procs.*, Fargo, USA, ISA, pp. 333-337.
- Lindström, L.I., C.N. Pellegrini, L.A.N. Aguirrezábal & L.F. Hernández (2006). Growth and development of sunflower fruits under shade during pre and early post-anthesis period. *Field Crops Research* 96: 151-159.
- Lindström, L.I., C.N. Pellegrini & L.F. Hernández (2007). Histological development of the sunflower pericarp as affected by pre and early post-anthesis canopy shading. *Field Crops Research* 103: 229-238.
- Logan, D.L. (2001). A First Course in the Finite Element Method Using Algor. Brooks-Cole, New York.
- Mauget, J.C., N. Boyer & J.L. Julien (1997). Responses of plant morphogenesis to mechanical stresses: an integrated approach. *Acta Horticulturae* 435: 231-232.
- Meyers, M.A. & K.K. Chawla (2009). Mechanical Behavior of Materials. 2nd ed. Cambridge University Press, Cambridge, England.
- Niklas, K.J. (1992). Plant Biomechanics. Univ. of Chicago Press, Chicago, USA.
- Preston, R.D. (1974). The Physical Biology of Plant Cell Walls.

- Chapman, London, England.
- Rasband, W.S. (2016). *ImageJ*, U. S. National Institutes of Health, Bethesda, Maryland, USA, URL: <https://imagej.nih.gov/ij/>.
- Ruzin, S.E. (1999). *Plant Microtechnique and Microscopy*. Oxford Univ Press, Oxford, England.
- Schneiter, A.A. & J.F. Miller (1981). Description of sunflower growth stages. *Crop Science* 21: 901-903.
- Sexton, R. & J.A. Roberts (1982). Cell biology of abscission. *Annual Review of Plant Physiology* 33: 133-162.
- Sulborska, A. (2013). Structure and distribution of glandular and non-glandular trichomes on above-ground organs in *Inula helenicum* L. (Asteraceae). *Acta Agrobotanica* 66: 25-34.
- Takeda, S., A. Iwasaki, N. Matsumoto, T. Uemura, K. Tatematsu & K. Okada (2013). Physical interaction of floral organs controls petal morphogenesis in *Arabidopsis*. *Plant Physiology* 161: 1242-1250.
- Tata, J.S. & H.C. Wien (2014). Anatomy of petal drop in sunflowers. *Journal of the American Society of Horticultural Science* 139: 669-675.
- Thibaut, B., J. Gril & M. Fournier (2001). Mechanics of wood and trees: some new highlights for an old story. *Comptes Rendus de l'Académie des Sciences, Serie II Fascicule B-Mécanique* 329: 701-716.
- Tholl, D. (2015). Biosynthesis and biological functions of terpenoids in plants. *Advances in Biochemical Engineering/Biotechnology* 148: 63-106.
- Wainwright, S.A., W.D. Biggs, J.D. Currey & J.M. Gosline (1982). *Mechanical Design of Organisms*. Princeton Univ. Press, Princeton, USA.
- White, P.J. & M.R. Broadley (2003). Calcium in plants. *Annals of Botany* 92: 487-511.
- Yilmaz, D., K. Ekinci, T. Dilmacunalb & S. Erbas (2011). Effect of harvesting hour on some physical and mechanical properties of *Rosa damascena* Mill. *Journal of the Science of Food and Agriculture* 91: 1585-1590.
- Zahra, A. (2012). Terpenoids and Gibberellic Acids Interaction in Plants. In: Montanaro G., Dichio B., (Eds.), pp. 345-364. *Advances in Selected Plant Physiology Aspects*, InTech, Ch. 16.